Microsyst Technol (2005) 11: 1214–1222
DOI 10.1007/s00542-005-0599-0

TECHNICAL PAPER

Babak A. Parviz · Khalil Najafi · Michael O. Muller
Luis P. Bernal · Peter D. Washabaugh

Electrostatically driven synthetic microjet arrays as a propulsion method for micro flight

Part I: principles of operation, modeling, and simulation

Received: 29 October 2004 / Accepted: 17 December 2004 / Published online: 26 July 2005

Abstract A novel propulsion method suitable for micromachining is presented that takes advantage of Helmholtz resonance, acoustic streaming, and eventually flow entrainment and thrust augmentation. In this method, an intense acoustic field is created inside the cavity of a Helmholtz resonator. Flow velocities at the resonator throat are amplified by the resonator and create a jet stream due to acoustic streaming. These jets are used to form a propulsion system. In this paper a system hierarchy incorporating the new method is described and the relevant governing equations for the Helmholtz resonator operation and acoustic streaming are derived. These equations can predict various device parameters such as cavity pressure amplitude, exit jet velocity and generated thrust. In a sample embodiment, an electrostatic actuator is used for generation of the initial acoustic field. The relevant design parameters for the actuator are discussed and an equivalent circuit model is synthesized for the device operation. The circuit model can predict the lowest order system resonance frequencies and the small signal energy conversion efficiency. A representative resonator performance is simulated and it is shown that velocities above 16 m/s are expected at jet nozzles. The calculated delivered thrust by this resonator with 0.7 μm diaphragm displacement amplitude is 3.3 μN at the resonance frequency.

List of symbols

A_{cor}	Area correction factor
A_D	Diaphragm area
A_E	Effective throat area
A_T	Geometric throat area
c	Speed of sound
d_0	Initial actuator gap
f	Frequency of operation
h_T	Throat height
L	Perforation hole depth
l	Perforation hole opening size
L_C	Diaphragm-throat distance
L_D	Diaphragm length
L_E	Equivalent inertia length of the throat
L_T	Geometric throat length
L_V	Equivalent viscous length of the throat
M	Distance between perforation holes
t	Diaphragm thickness
V_{bias}	DC bias voltage
V_{c0}	Initial cavity volume
μ	Air viscosity
σ	Diaphragm residual stress
ε_0	Permitivity of vacuum
ρ_{air}	Air density
ω_c	Cavity resonance frequency
ρ_D	Diaphragm density
ω_D	Diaphragm resonance frequency

B. A. Parviz (✉)
Department of Electrical Engineering, University of Washington,
Campus Box 352500, Seattle, WA 98195, USA
E-mail: babak@ee.washington.edu
Tel.: +1-206-6164038
Fax: +1-206-5433842

K. Najafi
Department of Electrical Engineering and Computer Science,
Center for Wireless Integrated Micro Systems,
University of Michigan, Ann Arbor, MI 48109-2122, USA

M. O. Muller · L. P. Bernal · P. D. Washabaugh
Aerospace Engineering Department, University of Michigan,
Ann Arbor, MI 48109-2122, USA

1 Introduction

Recent rapid progress in the field of Micro Electro Mechanical Systems (MEMS) has created a new opportunity for studying fluid dynamics in the micron scale by providing new actuation and sensing mechanisms. The ability to fabricate micro actuation mechanisms has led to the exploration of these actuators for the propulsion of micron-scale flying vehicles. In this paper, we aim to study the potential use of an array of synthetic

microjets as a means for thrust generation and propulsion for Micro Air Vehicles (MAV).

Aside from studies on insect flight (Weis-Fogh 1976; Nachtigall 1968; Brodsky 1994; Dalton 1975; Dickinson and Lighton 1995; Alexander 1995), investigating flight in the micro-scale has a short history. Crarey et al. (1992) suggested that building a micro flying machine was feasible considering the efficiency of MEMS actuators and energy storage content of solid-state batteries. As for potential applications, they suggested environmental monitoring, non-chemical pest control, studies of artificial life and artificial colonies, and personal robotics. For propelling such a micro flyer, both mimicking the flapping mechanism of insects and other approaches such as application of rotary propellers have been studied in the past few years. Externally actuated flapping wings (Shimoyama et al. 1994, 1995; Arai et al. 1995; Pornsin-Sirirak et al. 2000) and rotary wings covered by a magnetic layer (Miki and Shimoyama 2000) have demonstrated lift force generation. The external actuation mechanism necessary to operate these systems made them unsuitable for constructing an autonomous MAV with the exception of the design presented in (Pornsin-Sirirak et al. 2001). Other approaches to micro propulsion include the use of solid propellants in a digital micro propulsion system for small satellites (Lewis et al. 1999) and micro rockets (Lindsay et al. 2001; Teasdale et al. 2001), and a micro turbine that could potentially be used for thrust generation in a modified format (Lin et al. 1999). The main problems with combustion-based systems are excessive heat generation and operation at very high temperatures, which make them unsuitable for many applications. Also maintaining a large temperature gradient, essential for achieving high performance in a thermal system, is very difficult in small scale due to the large surface to volume ratio of structures. Attempts to build low temperature devices such as liquid vaporizing thrusters (Wallace et al. 1999) and micro fans (Kladitis et al. 2001) have yet to show sizable thrust generation.

In this paper we propose and study an alternative jet propulsion system suitable for application in a MAV. The propulsion system operates at low temperatures without rotary or sliding parts. It also does not require large relative displacements. These are all attractive features for simplifying the microfabrication process for making the system. The new propulsion system is based on generation of an acoustic field inside the cavity of a Helmholtz resonator and the subsequent momentum transfer due to acoustic streaming and flow entrainment and thrust augmentation. The focus of this paper is on developing correlations for performance of such a system and mainly dealing with the acoustic streaming and Helmholtz resonance phenomena. Assuming that the acoustic cavity is driven by an electrostatic actuator, we derive the basic governing fluidic, structural, and electrostatic equations that describe the system. These equations are summarized in the paper in order to provide a reference for future use in designing similar systems. The derived equations are also used to simulate the performance of a micromachined prototype. These equations form the basis for development of an equivalent circuit model for device operation and also establishment of design guidelines. Although our main goal is to study the merits of these jets for propulsion, many other applications of the microjet arrays can be envisioned such as flow control (Rathnasingham and Breuer 1997), cooling of integrated circuits (Chou et al. 2002; Stefanescu et al. 1999), and the use of the jets as components in micro chemical reactors for pumping and mixing (Wang and Menon 2001).

2 System overview

Figure 1 shows the hierarchy of the microjet generation array. An electrostatically actuated Helmholtz resonator forms the core of the system (Washabaugh et al. 2000). The Helmholtz resonator consists of a resonance chamber, throats and an oscillating diaphragm. The diaphragm is juxtaposed against a perforated electrode and is actuated electrostatically by application of a varying voltage between the electrode and the diaphragm. The oscillatory motion of the diaphragm creates an acoustic field inside the resonance chamber. The initial flow velocity is amplified by the resonator and forms a jet flow upon exiting the throat due to acoustic streaming. The exit jet flows of a few resonators are combined in an ejector shroud as shown in Fig. 1 to create a larger jet and achieve thrust

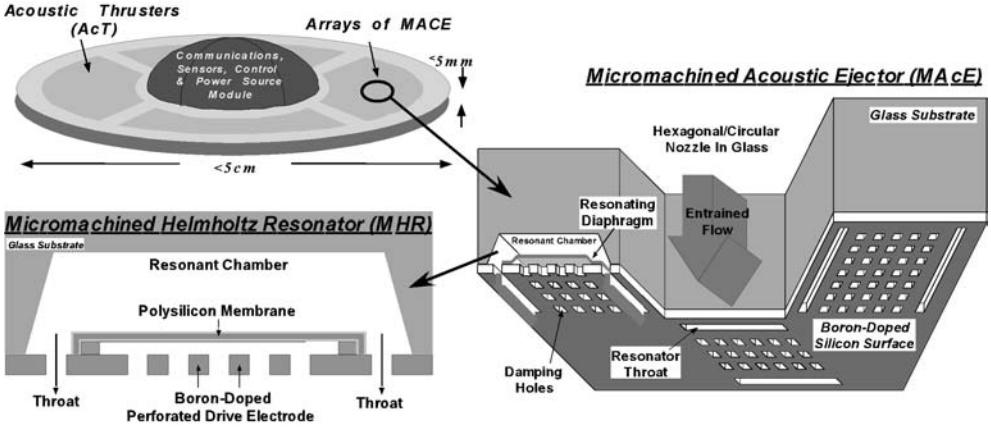

Fig. 1 Propulsion system hierarchy

augmentation by entraining more flow into the shroud (Bernal and Sarohia 1983). The placement of a few Helmholtz resonators around an ejector opening forms the Micromachined ACoustic Ejector (MACE). An array of MACEs can be used to form an ACoustic Thruster (ACT). In Fig. 1, four ACTs are used to propel and control a Micromachined Airborne Platform (MAP). Our goal here is to investigate the governing equations for the Helmholtz resonator and acoustic streaming and jet formation at the throat of the resonator. The performance of the MACEs and other higher-level system units will be presented in a future paper.

3 Acoustic streaming

Acoustic streaming constitutes the heart of the jet generation mechanism in the proposed propulsion scheme. In brief, it is the generation of jet streams by intense acoustic fields. This is a second order non-linear effect that can be caused by development of net forces due to Reynolds stresses correlated with loss mechanisms in the field (Lighthill 1978; Muller et al. 2000). Operating at relatively lower frequencies of about 1.3 kHz, micromachined synthetic jets producing exit velocities as high as 17 m/s have been demonstrated by M. Allen and coworkers (Coe et al. 1994, 1995). Initiation of streaming requires high velocity amplitude fluctuations for the fluid particles in the acoustic field (Smith and Glezer 1998). Efficient streaming in turn can transfer considerable momentum to the medium. In order to amplify the fluctuations generated by the MEMS actuator and initiate acoustic streaming, we have employed a Helmholtz resonator in our propulsion system.

4 Helmholtz resonator thrust generation through acoustic streaming

We propose a model that combines acoustic streaming and Helmholtz resonance and elucidates a correlation for the thrust generated by the system (Muller et al. 2000). The key assumptions are that the acoustic wavelength is much larger than system dimensions and that boundary layer separation at the throat exit causes a topological change of the stream lines. The justification for the later assumption is the synthetic jet results of (Coe et al. 1994, 1995) and others. These results cannot be explained by classical acoustic streaming theory, which assumes small amplitude oscillatory motion without topological change of the flow field. The conservation laws of fluid mechanics can be used to derive a model of the flow. The model can be cast in the form of inertia, compliance, damping and forcing terms. Inertia terms are associated with the air mass in oscillatory motion in the throat. Damping terms are caused by friction in the throat and orifice and by boundary layer separation effects. Acoustic radiation at the throat of the resonator also contributes to the loss of energy from the system. The compliance terms are associated with compressibility of the air mass in the resonator cavity. The forcing term results from the change of the cavity volume caused by the motion of the diaphragm.

4.1 Flow through the resonator throat

The line integral of the momentum equation along a streamline gives the equation relating the throat exit velocity to the pressure in the cavity. For the outflow part of the cycle, a typical streamline originates in the resonator cavity as shown in Fig. 2a. The line integral is evaluated between the cavity and the exit plane of the throat as shown in the figure. The flow is assumed to be incompressible. Thus (Muller 2002),

$$\rho \frac{\mathrm{d}}{\mathrm{d}t} \int \vec{u} \cdot \mathrm{d}\vec{s} + \rho \int \nabla \left[\frac{\vec{u}^2}{2} + \frac{P}{\rho} \right] \cdot \mathrm{d}\vec{s} = -\mu \int (\nabla \times \vec{\omega}) \cdot \mathrm{d}\vec{s} \tag{1}$$

The resulting equation after integration is

$$\frac{\mathrm{d}u_\mathrm{e}}{\mathrm{d}t} = \frac{1}{L_\mathrm{E}} \frac{P}{\rho} - \frac{u_\mathrm{e}^2}{2L_\mathrm{E}} - 8 \frac{\mu}{\rho} \frac{u_\mathrm{e}}{h_\mathrm{T}^2} \frac{L_\mathrm{V}}{L_\mathrm{E}} \quad u_\mathrm{e} \geqslant 0, \tag{2}$$

where $u_e(t)$ is the maximum velocity at the exit of the throat, $P(t) = P_c - P_{\mathrm{amb}}$ the relative pressure in the resonator cavity, and ρ (t) is the air density in the resonator cavity. For the inflow part of the cycle, typical

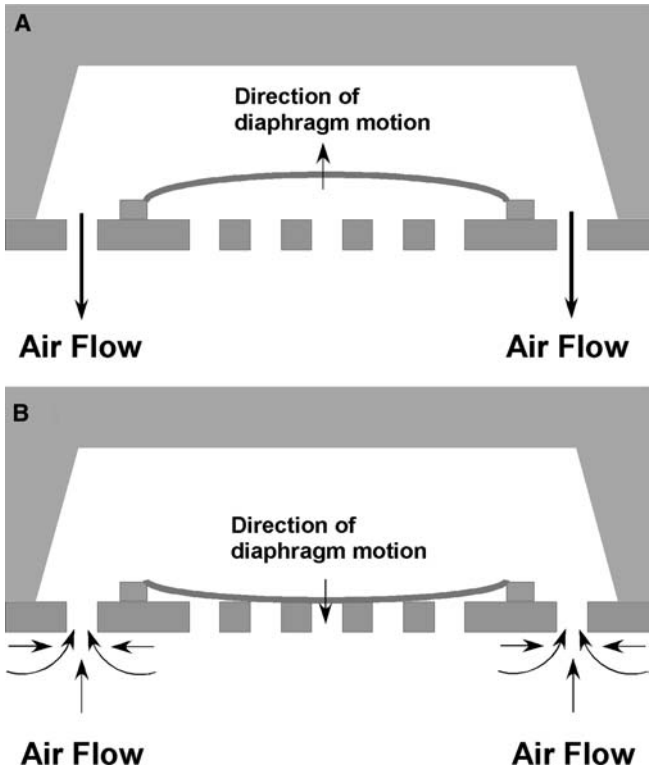

Fig. 2 **a** Outflow part of the cycle. **b** Inflow part of the cycle. Diaphragm motion is exaggerated for clarity. Not to scale

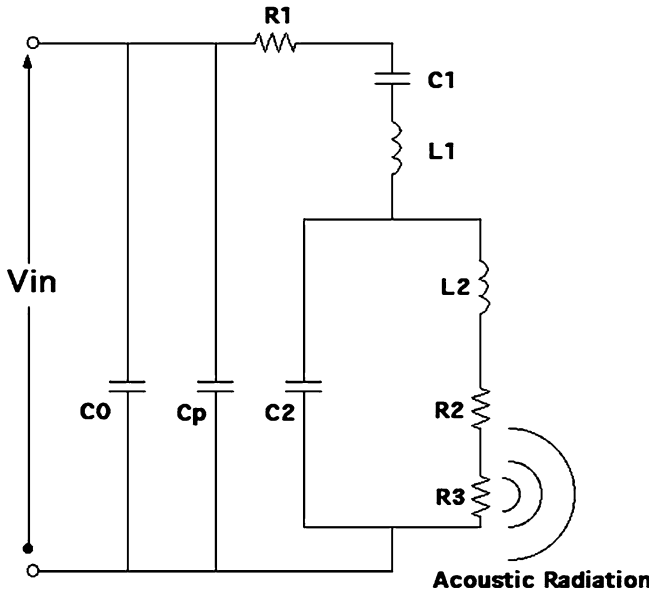

Fig. 3 The equivalent circuit model for the Helmholtz resonator

streamlines are shown in Fig. 3b. Boundary layer separation causes the pressure to be uniform at the throat–cavity interface and equal to the cavity pressure. In this case the line integral is evaluated between ambient conditions and the exit plane of the throat in the cavity giving

$$\frac{\mathrm{d}u_\mathrm{e}}{\mathrm{d}t} = \frac{1}{L_\mathrm{E}}\frac{P}{\rho_\mathrm{amb}} + \frac{u_\mathrm{e}^2}{2L_\mathrm{E}} - 8\frac{\mu}{\rho_\mathrm{amb}}\frac{u_\mathrm{e}}{h_\mathrm{T}^2}\frac{L_\mathrm{V}}{L_\mathrm{E}} \quad u_\mathrm{e}<0, \tag{3}$$

The numerical coefficients are valid only for a two-dimensional throat geometry (i.e. throat area $A_T \gg {h_T}^2$). It is also assumed that the equivalent L_E and L_V for the inflow and outflow parts of the cycle are equal. This is justified by the observation that these equivalent lengths scale with the geometrical length, L_T, and cross section area, A_T , of the throat. The equivalent inertia length of the throat is given by

$$L_\mathrm{E} = L_\mathrm{T} + \frac{(\pi A_\mathrm{T})^{1/2}}{4} \tag{4}$$

The second term in this equation accounts for the inertia of the air mass moving inside the resonator cavity.

Damping is associated with the last two terms of Eqs. 2 and 3. The first term is proportional to the square of the exit velocity and is due to flow separation at the throat exit. Friction in the throat is characterized by L_V, the equivalent viscous length of the throat. The magnitude of L_V is determined by the resonator geometry and Reynolds number.

4.2 Cavity compliance

The resonator cavity compliance and the forcing term are obtained by considering conservation of mass in the cavity.

$$\frac{\mathrm{d}}{\mathrm{d}t}(\rho V_\mathrm{c}) = -\rho u_\mathrm{e} A_\mathrm{E} \tag{5}$$

where A_E is the effective area of the throat and V_c is the cavity volume. The streamline topology changes discussed above imply that the air density in the throat is different during the inflow and outflow parts of the cycle. It follows assuming isentropic compression of the air mass in the cavity,

$$\frac{\mathrm{d}P}{\mathrm{d}t} = c^2\frac{\mathrm{d}\rho}{\mathrm{d}t} = -\rho c^2\frac{u_\mathrm{e}A_\mathrm{E}}{V_\mathrm{c}} - \rho c^2\frac{1}{V_\mathrm{c}}\frac{\mathrm{d}V_\mathrm{c}}{\mathrm{d}t} \quad u_\mathrm{e}\geqslant 0, \tag{6}$$

$$\frac{\mathrm{d}P}{\mathrm{d}t} = c^2\frac{\mathrm{d}\rho}{\mathrm{d}t} = -\rho_\mathrm{amb} c^2\frac{u_\mathrm{e}A_\mathrm{E}}{V_\mathrm{c}} - \rho c^2\frac{1}{V_\mathrm{c}}\frac{\mathrm{d}V_\mathrm{c}}{\mathrm{d}t} \quad u_\mathrm{e}<0, \tag{7}$$

where c is the speed of sound. The effective area of the throat, A_E, is always less than the geometrical area, A_T, because of the viscous effects. At high Reynolds numbers, $A_E \cong A_T$. There is only a small correction due to the thin viscous region near the wall (Ekman boundary layer). At low Reynolds numbers the viscous effects dominate. A parabolic velocity profile develops in the throat which gives $A_E = 2/3\ A_T$ for a two-dimensional throat geometry.

4.3 Thrust generation

The thrust produced by the Helmholtz resonator can be evaluated by considering conservation of momentum for the flow outside the resonator. The time integral of the momentum flux divided by the period of oscillation gives a positive contribution to the mean thrust

$$J = \frac{1}{T}\int_{u_\mathrm{e}>0}\int_{A_\mathrm{T}} \rho u^2 \mathrm{d}A\mathrm{d}t = \frac{1}{T}\int_{u_\mathrm{e}>0} \rho u_\mathrm{e}^2 A_\mathrm{JE}\mathrm{d}t \tag{8}$$

where T is the period of oscillation, and A_{JE} is the effective area of the throat for thrust. At high Reynolds numbers, the effective area of the throat equals the geometrical area except for boundary layer effects, which are generally small, i.e. $A_{JE} = A_T$.

4.4 Acoustic radiation

An important means for the transfer of energy out of the Helmholtz resonator system especially at low amplitudes of oscillation is acoustic radiation. In order to incorporate this into the model, the displacement of a fluid element at the throat of the Helmholtz resonator, ξ, can be considered. If viscous losses are negligible, the equation describing this displacement is (Kinsler et al. 1982):

$$m\frac{\mathrm{d}^2\xi}{\mathrm{d}t^2} + R_\mathrm{r}\frac{\mathrm{d}\xi}{\mathrm{d}t} + s\xi = A_\mathrm{E}Pe^{j\omega\mathrm{t}} \tag{9}$$

In which m is the effective mass of the fluid in the throat, R_r the term describing the acoustic radiation, s is the stiffness of the cavity and the right hand side of the equation describes the forcing term on the system. After differentiating Eq. 9:

$$m\frac{\mathrm{d}^2u_\mathrm{e}}{\mathrm{d}t^2}+R_\mathrm{r}\frac{\mathrm{d}u_\mathrm{e}}{\mathrm{d}t}+su_\mathrm{e}=\frac{\mathrm{d}}{\mathrm{d}t}\left(A_\mathrm{E}Pe^{j\omega t}\right) \tag{10}$$

clearly the second term on the left hand side acts as a damper. In the absence of external forcing, this causes the exit velocity to approach zero after a few cycles. If it is assumed that a fluid element oscillates harmonically in the throat of the resonator and the throat radiates sound into the surroundings as an open-ended pipe, for the terminal radiation impedance of a baffled piston with area A_E, one can write (Kinsler et al. 1982):

$$\begin{aligned}R_\mathrm{r}&=A_E\rho_0c\left(1-\frac{2J_1\left(\frac{2\omega a}{c}\right)}{\frac{2\omega a}{c}}\right)\\&=A_E\rho_0c\left[\frac{1}{2^2 1!2!}\left(\frac{2\omega a}{c}\right)^2-\frac{1}{2^4 2!3!}\left(\frac{2\omega a}{c}\right)^4+\cdots\right]\end{aligned} \tag{11}$$

$$\begin{aligned}X_\mathrm{r}&=\frac{4A_\mathrm{E}\rho_0c}{\pi}\\&\times\left[\frac{1}{3}\left(\frac{2\omega a}{c}\right)-\frac{1}{3^2.5}\left(\frac{2\omega a}{c}\right)^3+\frac{1}{3^2.5^2.7}\left(\frac{2\omega a}{c}\right)^5-\cdots\right]\end{aligned} \tag{12}$$

in which ω is the angular frequency of the wave, a the radius of the opening and J_1 is the first order Bessel function. When $\omega\, a \ll c$, which is the case for most micro systems due to their small dimensions, the above equations can be approximated by

$$R_\mathrm{r}=\frac{\rho_0\omega^2A_\mathrm{E}^2}{2\pi c} \tag{13}$$

$$X_\mathrm{r}=\frac{8}{3}\rho_0\omega\sqrt[3]{\frac{A_\mathrm{E}}{\pi}} \tag{14}$$

The radiation reactance acts as mass loading for the system and can be neglected without introducing a large error in most cases. The resistance term, R_r, can be used to determine the energy loss due to radiation.

5 System modeling

Using the above equations, the performance of a prototype micro propulsion system utilizing a Helmhotlz resonator can be modeled. Our candidate resonator unit is shown in Fig. 2. The initial acoustic field in the resonance chamber is generated by an electrostatic actuator. We begin with outlining the important design aspects of the electrostatic actuator and then present the complete modeling results.

5.1 The electrostatic actuator

The electrostatic actuator in this system consists of two conductive parallel plates. One of the plates is perforated to reduce damping. The electrostatic attraction force between the plates, $F(d)$, can be written as:

$$F(d)=-\frac{1}{2}\varepsilon_0V^2\frac{A_\mathrm{eff}}{d^2} \tag{15}$$

in which d is the distance between the two plates, ϵ_0 the permitivity of the vacuum and A_eff is the effective area of the plate. For perforated plates, if the fringing fields are neglected, A_eff is be the total area minus the area of perforations. If the perforated plate is stationary and the other plate (the diaphragm) is under high tension, a simple equation of motion for the diaphragm can be written as:

$$\rho_\mathrm{D}t_\mathrm{D}\frac{4A_\mathrm{D}}{\pi^2}\left(\frac{\mathrm{d}^2h}{\mathrm{d}t^2}+\omega_\mathrm{D}^2h\right)=-F(d) \tag{16}$$

in which A_D is the area of the diaphragm, t_D the thickness, h the center deflection, ρ_D the density, and ω_D is related to the resonance frequency of a square diaphragm as:

$$\omega_\mathrm{D}=2\pi f_{11}=\pi\sqrt{\frac{2\sigma}{\rho_\mathrm{D}A_\mathrm{D}}} \tag{17}$$

Acoustic streaming based propulsion systems should operate at high frequencies and thus the diaphragm tension (σ) in the above formula assumes a large value.

5.2 Air damping in the electrostatic actuator

The effect of the air flow in the actuator gap and perforations has two components, one acting as a damper and the other as a spring (Chen and Yao 1996; DaSilva et al. 1999; Minami et al. 1999). Exact modeling of this effect requires finite element simulations; however, a simple model can be used to investigate the damping effect to the first order (Skvor 1967). If the flow through the perforations and the gap is considered to be laminar and incompressible, the damping force can be divided to two components. One is due to the flow parallel to the plates in the gap and the other is due to the flow inside the perforations. The pressure required to force the air through the gap for one hole of the perforation can be written as (Skvor 1967):

$$P_\mathrm{D1}=\frac{3(1.13)^2\mu M^2B}{d^3}\frac{\mathrm{d}h}{\mathrm{d}t} \tag{18}$$

with

$$B(S)=\frac{1}{4}\ln\left(\frac{1}{S}\right)-\frac{3}{8}+\frac{1}{2}S-\frac{1}{8}S^2 \tag{19}$$

$$S=\frac{l^2}{\frac{\pi}{4}(1.13)^2M^2} \tag{20}$$

in which μ is the viscosity of air, M the center to center distance between the holes in the perforation, d the distance between the two plates, h the center deflection, and l is the size of the square perforation hole. If the air flow through the holes is approximated as fully developed pipe flow (Olsen and Wright 1990), the pressure required to move the volume of air per hole, or the second component of damping can be written as

$$P_{D2} = \frac{32\mu L}{l^2}\frac{dh}{dt} \tag{21}$$

in which L is the depth of the perforation hole. Fully developed pipe flow is not a valid assumption for a general case; however, it provides a good approximation of the flow for the design that is simulated in the next section considering the aspect ratio of the openings. By using Eq. 21, the total damping pressure can be written as the sum of the two components:

$$P_D = \frac{4}{\pi^2}(P_{D1} + P_{D2}) \tag{22}$$

The preceding coefficient is for correction due to the non-planar shape of the bent plate. For a constant $A_r = l^2/M^2 = \text{cte}$, S and $B(S)$ are constants and thus damping pressure can be written:

$$P_D = \left(\frac{3(1.13)^2\mu B(S(A_r))}{d^3}\frac{A_r}{l^2} + 32\frac{\mu L}{l^2}\right)\frac{dh}{dt} \tag{23}$$

To find the optimum size of l

$$\frac{\partial}{\partial l}P_D = 0 \tag{24}$$

thus $l_{optimum}$ can be derived as

$$l_{optimum} = \sqrt[4]{\frac{32Ld^3A_r}{3(1.13)^2B(S(A_r))}} \tag{25}$$

Note that B should always assume a positive value.

5.3 Small signal equivalent circuit model

A small signal equivalent circuit model can be derived for the device at the onset of streaming. In this model it is assumed that the main mechanism for energy transfer from the device is acoustic radiation. By using equations 2, 6, 13, 15, 16, 18 and 21, the transfer function in the S domain for an equivalent circuit presentation can be written as:

$$I = C_0SV_\Delta + \frac{\frac{2C_0P_{E0}}{d_0\rho_D t}SV_\Delta}{S^2 + \frac{\pi^2 b_d}{4\rho_D t}S + \{\ldots\}} \tag{26}$$

$$\{\ldots\} = -\frac{\frac{\rho L_E\omega_c^4 A_D}{A_E\rho_D t}}{S^2 + (b_{cv} + b_{cr})S + \omega_c^2} + \omega_D^2 - \frac{2P_{E0}}{\rho_D t d_0} + \frac{\rho L_E A_D}{\rho_D t A_E}\omega_c^2$$

This can be synthesized to form the circuit shown in Fig. 3. C_p is the parasitic capacitance associated with the structure. The other circuit elements are defined as:

$$C_0 = \frac{\varepsilon_0 A_D A_{cor}}{d_0} \tag{27}$$

$$L_1 = \frac{d_0^2\rho_D t A_D}{C_0^2 V_{bias}^2} \tag{28}$$

$$C_1 = \frac{\frac{1}{L_1}}{\omega_D^2 - \frac{2P_{E0}}{\rho_D t d_0}} = \frac{\frac{1}{L_1}}{\frac{2\sigma\pi^2}{\rho_D A_D} - \frac{\varepsilon_0 A_{cor}V_{bias}^2}{d_0^3\rho_D t}} \tag{29}$$

$$R_1 = L_1\left(\frac{1}{\rho_D t}\right)\frac{32\mu L}{l^2} + \frac{3(1.13)^2\mu M^2}{d_0^3} \times\left(\frac{1}{4}\ln\frac{\pi/4(1.13)^2M^2}{l^2} - 3/8 + \frac{2l^2}{\pi(1.13)^2M^2} - \frac{2l^4}{\pi^2(1.13)^4M^4}\right) \tag{30}$$

$$C_2 = \frac{\rho_D t V_{c0}}{\rho_{air}A_D c^2 L_1} \tag{31}$$

$$L_2 = \frac{1}{\omega_c^2 C_2} = L_1\frac{\rho_{air}L_E A_D}{\rho_D t A_E} \tag{32}$$

$$R_2 = L_2\frac{8\mu L_V}{\rho_{air}L_E h_T^2} \tag{33}$$

$$R_3 = L_2\frac{2\pi A_E}{cL_E}f^2 \tag{34}$$

$$P_{E0} = \frac{1}{2}\frac{\varepsilon_0 A_{cor}V_{bias}^2}{d_0^2} \tag{35}$$

P_{E0} is the electrostatic force between the actuator plates prior to deflection and appears in the equations as a result of linearization of the forcing term. Here it is assumed that the input voltage consists of a large DC component V_{bias} and a small AC component V_Δ.

Two important resonance phenomena interact in the complete system. The cavity Helmholtz resonance that is signified by ω_c and the diaphragm resonance shown by ω_D. The first LC tank in the circuit with L_1 and C_1 has a resonance frequency very close to the diaphragm resonance frequency but shifted by a bias dependant factor:

$$\omega_1 = \sqrt{\omega_D^2 - \frac{\varepsilon_0 A_{cor}}{d_0^3\rho_D t}V_{bias}^2} \tag{36}$$

The bias voltage lowers the resonance frequency and thus effectively "softens" the spring constant of the diaphragm. The other important resonance frequency in the system, ω_c, is directly matched with the resonance frequency of the L_2 and C_2. However, due to the presence of the frequency dependent resistance $R3$, the resonance frequency of the whole LC tank does not match the resonance frequency derived from L_2 and C_2.

Table 1 Helmholtz resonator structure data

Parameter	Value
Diaphragm area	1200 × 1200 μm
Diaphragm thickness	1.8 μm
Diaphragm residual stress	79.44 MPa
Diaphragm resonance frequency	104.7 kHz
Chamber depth	35 μm
Chamber length	1730 μm (effective)
Chamber width	1350 μm
Throat length	15 μm
Throat height	15 μm
Throat width	1406 μm (effective)
Helmholtz resonance frequency	59.1 kHz
No. of throats	2

It is very important to note that although the system has two distinct resonance frequencies that do not inevitably match, in general the maximum power delivery of the system appears at a frequency in between the two. An example follows shortly. The resistors in the circuit, model the loss of energy from the device as expected. R_1 is related to the losses due to flow through perforations and R_2 models the viscous losses in the cavity. In the model, the radiation element is shown as a frequency dependant resistor R_3. The power consumed on this resistor shows the output power of the system at low frequencies.

6 Simulation results

Both the small signal model and direct solution of the differential equations with MATLAB were used to simulate the behavior of the propulsion system. The typical parameters for the simulated device where chosen to match fabricated micromachined devices described in Parviz et al. (2005) (Table 1). Assuming 0.7 μm diaphragm displacement the system differential equations can be numerically solved to yield the exit jet flow velocity as shown in Fig. 4. This system has the cavity resonance frequency of 59.1 kHz and diaphragm mechanical resonance frequency of 104.7 kHz. Figure 5 shows the calculated acoustic power output of a resonator. As expected the system has two peaks, one at 50 kHz and one at 175 kHz. Note that these peaks do not coincide with the two intrinsic resonance frequencies of the system, ω_c and ω_D. Figure 6 shows the calculated energy delivery efficiency of the system. This curve has only one peak (32% at 115 kHz) that is located close to the resonance frequency of the diaphragm. This suggests that for small amplitude actuations, the efficiency is mainly determined by the diaphragm rather than the cavity. For a good and efficient design, the two resonance points of the system should be designed to be as close as possible so that the maximum efficiency point can be close to a maximum point for the output power.

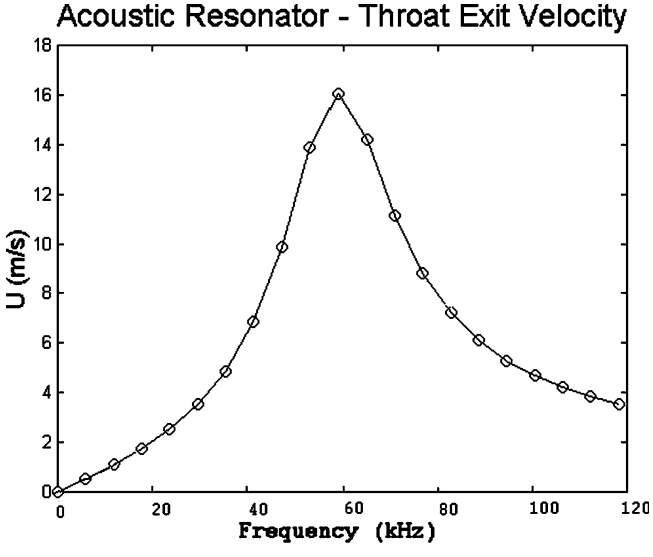

Fig. 4 Calculated output jet velocity as a function of frequency for 0.7 μm displacement of the diaphragm

7 Conclusions

We have introduced a novel propulsion system based on acoustic streaming. The propulsion system takes advantage of the Helmholtz resonance effect to generate high flow oscillation velocities. These oscillations are converted to a microjet through acoustic streaming and are used to generate thrust. A candidate architecture for fabrication of a microjet array is suggested using a high frequency electrostatic actuator to generate the initial acoustic field in the resonance cavity. This embodiment does not have sliding or rotary parts and does not require large relative displacements. These are all attractive features and simplify the microfabrication of the device.

We have derived the governing flow equations for this device. We have also considered the relevant structural and electrostatic equations for the MEMS electrostatic actuators that drive the acoustic cavities. Damping forces play a critical role in the operation of the electrostatic actuator. An optimum design exists for perforations on the actuator back plate to minimize the air damping effect if linear and flat motion of the diaphragm is considered. Equation 25 depicts this value.

Numerical solution of the governing equations can be used to predict various system parameters such as pressure fluctuations in the Helmholtz resonator cavity, output flow velocity, thrust, and equivalent flow lengths. In order to combine the electrostatic, fluidic and structural mechanics effects in the device in a unified model, an equivalent circuit model is synthesized based on the governing equations. Small signal energy conversion efficiency of the system can be found by simulating the equivalent circuit model and calculating the power consumption on elements representing viscous losses and radiation in the system. A sample device is simulated and it is shown that jet exit velocities exceeding 16 m/s can be generated. This device had two

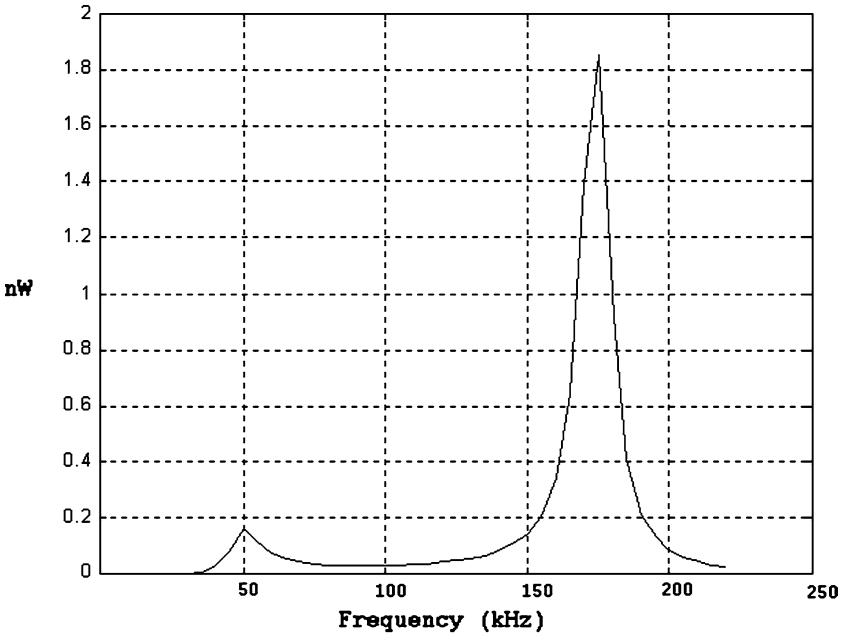

Fig. 5 Acoustic power delivered by the system versus its operating frequency, simulated using the equivalent small signal circuit model

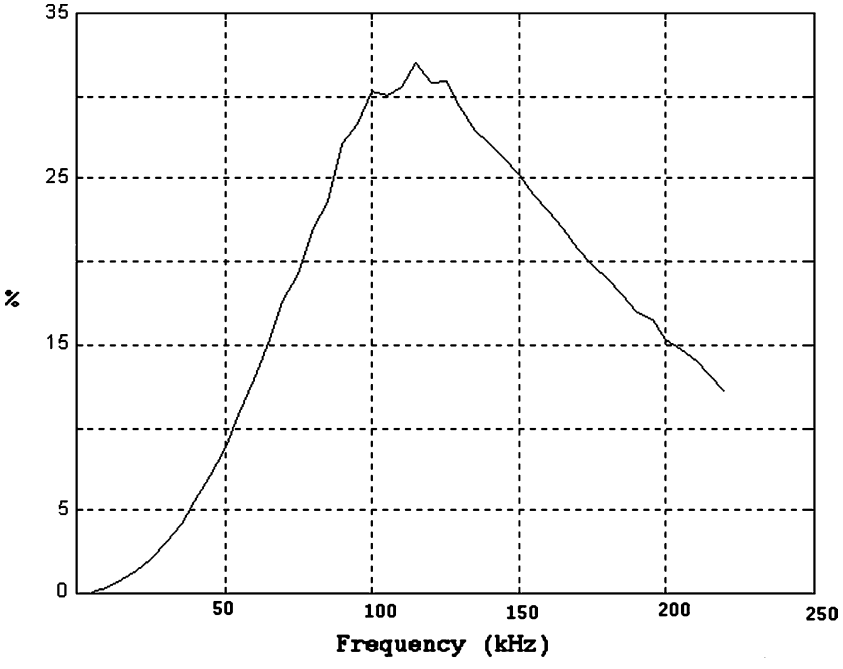

Fig. 6 System efficiency as a function of the system operation frequency, simulated using the equivalent small signal circuit model

resonance frequencies at 50 and 175 kHz and had a 32% maximum energy conversion efficiency for small signal operations.

Acknowledgements The authors would like to thank the Defense Advanced Research Projects Agency (DARPA) for providing the support for this work through contract# N00019-98-K-0111. The help of Christopher Morris in the preparation of the manuscript is appreciated.

References

Alexander RM (1995) Springs for wings. Science 268:50–51

Arai KI, Sugawara W, Honda T (1995) Magnetic small flying machines. In: Proceedings of Eurosensor IX. Stockholm, Sweden, pp 316–319

Bernal LP, Sarohia V (1983) Entrainment and mixing in thrust augmenting ejectors. In: AIAA 21st aerospace science meeting. Reno, Nevada

Brodsky AK (1994) The evolution of insect flight. Oxford University Press, Oxford

Chen CL, Yao JJ (1996) Damping control of MEMS devices using structural design approach. In: Proceedings of the solid state sensor and actuator workshop. Hilton Head, South Carolina, pp 72–75

Chou T, Najafi K, Muller M, Bernal L, Washabaugh P, Parviz BA (2002) Micromachined e-jet for IC-chip cooling. In: Technical digest of the IEEE international solid-state circuits conference, pp 356–357

Coe DJ et al (1994) Micromachined jets for manipulation of macro flows. In: Solid-state sensor& actuator workshop digest. Hilton Head, SC, pp 243–247

Coe DJ et al (1995) Addressable micromachined jet arrays. In: Proceedings of the transducers '95. Stockholm, Sweden, pp 329–332

Crarey SB et al (1992) Prospects for microflight using micromechanisms. In: Proceedings of international symposium on theory of machines and mechanisms. Nagoya, Japan, pp 273–275

Dalton SN (1975) Borne on the wind: the extraordinary world of insects in flight. Reader's Digest Press, UK

DaSilva MG et al (1999) Gas damping and spring constant effects on MEMS devices with multiple perforations and multiple gaps. In: Proceedings of the transducers 99. Sendai, Japan, pp 1148–1151

Dickinson MH, Lighton JRB (1995) Muscle efficiency and elastic storage in the flight motor of drosophila. Science 268:87–90

Kinsler LE, Frey AR, Coppens AB, Sanders JV (1982) Fundamentals of acoustics, 3rd edn. Wiley, New York

Kladitis PE et al (2001) Solder self-assembled micro axial flow fan driven by a scratch drive actuator rotary motor. In: Proceedings of the 14th IEEE MEMS conference. Interlaken, Switzerland, pp 598–601

Lewis DH, Janson SW, Cohen RB, Antonsson EK (1999) Digital micropropulsion. In: Proceedings of the 12th IEEE MEMS Conference. Orlando, FL, pp 517–522

Lighthill J (1978) Acoustic streaming. J Sound Vib 61:391–418

Lin CC et al (1999) Fabrication and characterization of a micro turbine/bearing rig. In: Proceedings of the 12th IEEE MEMS conference. Orlando, FL, pp 529–533

Lindsay W et al (2001) Thrust and electrical power from solid propellant micro rockets. In: Proceedings of the 14th IEEE MEMS conference. Interlaken, Switzerland, pp 606–610

Miki N, Shimoyama I (2000) A micro-flight mechanism with rotational wings. In: Proceedings of the 13th IEEE MEMS conference. Miyazaki, Japan, pp 158–163

Minami K et al (1999) Simple modeling and simulation of the squeeze film effect and transient response of the MEMS device. In: Proceedings of the 12th IEEE MEMS conference. Orlando, Florida, pp 338–343

Muller MO et al (2000) Thrust performance of micromachined synthetic jets. In: AIAA fluids 2000 conference. Denver, Colorado, paper 2000–2404

Muller MO et al (2000) Micromachined acoustic resonators for microjet propulsion. In: AIAA fluids conference. Reno, Nevada, paper 2000–00547

Muller MO (2002) Flow structure, performance, and scaling of acoustic jets. PhD Dissertation, University of Michigan

Nachtigall W (1968) Insects in flight. McGraw-Hill Inc, NY

Olsen RM, Wright SJ (1990) Essentials of engineering fluid mechanics, 5th edn. Harper and Row Publishers, New York

Parviz BA, Najafi K, Muller MO, Bernal LP, Washabaugh PD (2005) Electrostatically driven synthetic microjet arrays as a propulsion method for micro flight. Part II: microfabrication and initial characterization. Microsyst Technol DOI 10.1007/s00542-005-0600-y

Pornsin-Sirirak TN, Lee SW, Nassef H, Grasmeyer J, Tai YC, Ho CM, Keennon M (2000) MEMS wing technology for a battery-powered ornithopter. In: Proceedings of the 13th IEEE MEMS conference. Miyazaki, Japan, pp 799–804

Pornsin-sirirak TN, Tai YC, Nassef H, Ho CM (2001) Titanium-alloy MEMS wing technology for a micro aerial vehicle application. Sens Actuators A89:95–103

Rathnasingham R, Breuer KS (1997) Coupled fluid-strcutural characteristics of actuators for flow control. AIAA J 35:832–837

Shimoyama I, Kubo Y, Kaneda T, Miura H (1994) Simple microflight mechanism on silicon wafer. In: Proceedings of the 7th IEEE MEMS workshop. Oiso, Japan, pp 148–152

Shimoyama I, Fujisawa YK, Getzan GD, Miura H, Shimada M, Matsumoto Y (1995) Fluid dynamics of microwing. In: Proceedings of the 8th IEEE MEMS conference. Amsterdam, Netherlands, pp 380–385

Skvor Z (1967) Acoustical resistance of electrostatic transducers. Acustica 19:295–299

Smith BL, Glezer A (1998) The formation and evolution of synthetic jets. Phys Fluids 10:2281–2297

Stefanescu S, Mehregany M, Leland J, Yerkes K (1999) Micro jet array heat sink for power electronics. In: Technical digest of the 12th IEEE international conference on MEMS. Orlando, FL, pp 165–170

Teasdale D, Milanovic V, Chang P, Pister KSJ (2001) Microrockets for smart dust. Smart Mater Struct 10:1145–1155

Wallace AP et al (1999) Design, fabrication and demonstration of a vaporizing liquid attitude control microthruster. In: Proceedings of transducers '99. Sendai, Japan, pp 1800–1803

Wang H, Menon S (2001) Fuel-air mixing enhancement by synthetic microjets. AIAA J 39:2308–2319

Washabaugh PD et al (2000) An approach toward a wafer integrated micro air vehicle. In: Proceedings of the 15th Bristol international conference on unmanned air vehicle systems. Bristol, United Kingdom, 33.1–33.12

Weis-Fogh T (1976) Energetics and aerodynamics of flapping flight: a synthesis. Insect flight. Blackwell Scientific Publications, Oxford, pp 49–72